Step Shear Dynamics of Entangled Polymer Liquids

Javier Sanchez-Reyes and Lynden A. Archer*

School of Chemical Engineering, Cornell University, Ithaca, New York 14850

Received March 1, 2002; Revised Manuscript Received April 19, 2002

ABSTRACT: Nonlinear step shear dynamics of entangled solutions of an ultrahigh molecular weight polystyrene (PS20M, $\overline{M}_w = 20.06 \times 10^6$ g/mol) in diethyl phthalate (DEP) are investigated. PS20M/DEP solutions with concentrations ϕ spanning the range from marginally entangled to highly entangled liquids are used to quantify the effect of entanglement density on dynamics. Step shear measurements are performed in a setting where errors due to interfacial slip can be determined and minimized. Two characteristic "separability" times $\lambda_{k1} = (16.5 \pm 4.7)\tau_{Rouse}$ and $\lambda_{k2} \gg \tau_{Rouse}$ are identified, beyond which nonlinear shear relaxation moduli $G(\gamma,t) = \sigma(\gamma,t)/\gamma$ can be factorized into separate time-dependent $G(t)$ and strain-dependent $h(\gamma)$ functions. Contrary to expectations from theory, both separability times are stronger functions of polymer concentration ($\lambda_{k1} \sim \phi^{0.7}$, $\lambda_{k2} \sim \phi^{3.2}$) than expected for a pure Rouse stretch relaxation route to factorability, $\lambda_k \propto \tau_{Rouse} \sim \phi^0$. On the other hand, we find that a single shear damping function, $h(\gamma)$, close to the universal damping function h_{DE-IA} predicted by Doi−Edwards theory accurately describes the strain dependence of step shear material response, irrespective of PS20M/DEP entanglement density.

1. Introduction

Relaxation dynamics of polymer liquids following imposition of step shear deformations is a subject of longstanding importance in polymer science. For small strain amplitudes γ, the time-dependent shear modulus following step strain $G(t) = \sigma(t)/\gamma$ is independent of shear strain and is a unique function for a given polymer liquid. Relaxation moduli $G(t)$ measured in small-amplitude step shear may therefore be used to calculate other material specific characteristics, such as the frequency dependence of storage $G'(t) \equiv \omega \int_0^\infty \sin(\omega t) \cdot G(t)\, dt$ and loss moduli $G''(t) \equiv \omega \int_0^\infty \cos(\omega t) G(t)\, dt$ and the zero-shear viscosity $\eta_0 = \int_0^\infty G(t)\, dt$.[1,2] At higher shear strains, the shear relaxation modulus is a nonlinear function of strain $G(t,\gamma) = \sigma(t,\gamma)/\gamma$ and generally cannot be simply related to other viscoelastic functions. For fluids in the class entangled linear polymers, the theory of Doi and Edwards contends that $G(t,\gamma) = G(t) \cdot h_{DE}(\gamma)$; $t > \lambda_k$,[2] where $G(t) = G_N \sum_{p;odd} (8/[(\pi p)^2]) \exp[-p^2 t/\tau_d]$, $h_{DE}(\gamma)$ is a universal function of strain, and the *separability time* λ_k is a unique time of order 4−5 times the longest Rouse relaxation time $\tau_{Rouse} = (6/\pi^2)\tau_m N^2$. Here, $N = M/M_0$ is the degree of polymerization, and τ_m is the longest segmental relaxation time.

After nearly 4 decades of active research by several investigators, it is now generally accepted that the step shear *damping function* $h(\gamma)$ for weak-to-moderately entangled polymer liquids is close to the universal function $h_{DE}(\gamma)$ predicted by Doi and Edwards.[2−6] The separability time is somewhat larger than the prediction, however, approaching the terminal or reptation relaxation time $\tau_d \approx 6\tau_{Rouse}(N/N_e)^{1.5\pm0.2}$ in many polymer systems.[6,7] The situation in well-entangled polymer systems is far more complicated. In these systems various levels of discrepancy have been reported between damping functions predicted by theory and determined from experiment.[4−11] Curiously, discrepancies are often found to be largest at low strains, outside the linear viscoelastic regime.[5−7] Moreover, although $G(t,\gamma)$ can in most cases be factorized into separate strain and time-dependent functions, the path to factorability is a rather complicated function of strain, and the factorability time more closely aligned with τ_d than with τ_{Rouse}.[6,7] These discrepancies have led to recent speculation that the damping function may not be universal for fluids belonging to the class entangled, linear polymers.

A common theme in many of the studies where negative deviations from $h_{DE}(\gamma)$ have been reported is that instrument, interfacial, and/or bulk material artifacts might be to blame for the observations. Attempts to systematically isolate and remove these effects have, to date, only served to reinforce the view that the observed differences are perhaps real.[6] Recently, Sanchez-Reyes and Archer performed a detailed study of wall slip in steady-state shear flow of entangled polymer solutions similar to those where the largest deviations from $h_{DE}(\gamma)$ have been reported.[11] These authors found measurable levels of slip in these systems at all Weissenberg numbers $Wi = \dot{\gamma}\tau_d$, but the slip was largest at Wi values between 0.1 and 10, i.e., in a similar range to the shear strain values where the largest deviations from $h_{DE}(\gamma)$ have been reported.[7,9] Sanchez-Reyes and Archer also reported that while surface treatments using simple sand-blasting methods can reduce the severity of slip, this method does not generally provide significant improvement over the untreated case. The authors instead found that if shear surfaces were pretreated by grafting a single layer of micron-sized glass beads, slip could be dramatically reduced for bead diameters as low as 3−5 μm (the lowest diameters studied). This finding suggests that slip errors can be minimized in any polymer liquid by appropriately tuning surface roughness levels of the measurement fixtures.

In the present study we investigate nonlinear step shear dynamics of entangled polymer liquids spanning a broad range of entanglement density. We focus in particular on the effect of polymer entanglement density N/N_e on the nonlinear relaxation modulus $G(t,\gamma)$ in systems where errors due to wall slip have been removed. The study is facilitated by rheometry measurements using large-diameter cone-and-plate fixtures

10.1021/ma020321q CCC: $22.00
Published on Web 05/24/2002

Table 1. Physical Properties of PS/DEP Solutions Used in This Study

solution	ϕ	N/N_e	η_0 (Pa·s)	G_e (Pa)	τ_d (s)	λ_{k1} (s)	λ_{k2} (s)	τ_R (s)[a]
PS20M1.5%	0.015	4	23.6	12.5	6.75 ± 0.5	7.6 ± 0.6	6.4 ± 1.3	0.73
PS20M2.5%	0.025	8	2.87×10^2	39.8	18.8 ± 1.3	9.5 ± 1.1	7.6 ± 0.5	0.85
PS20M3%	0.033	11	1.09×10^3	74.4	52.4 ± 4.8	7.9 ± 1.7	64.0 ± 15.7	0.9
PS20M4%	0.046	18	3.05×10^3	167.4	87.1 ± 9.7	10.8 ± 0.6	136.1 ± 24.9	0.55
PS20M5%	0.053	22	1.35×10^4	226.9	198.3 ± 31	15.9 ± 5.3	213.2 ± 41.6	1.27
PS20M6%	0.065	29	2.9×10^4	363.1	468.4 ± 23	12.0 ± 1.8	281.4 ± 63.5	1.06
PS20M8%	0.079	37	8.37×10^4	590.8	590.3 ± 47	22.5 ± 5.1	988.8 ± 184.9	1.25

[a] τ_R = longest Rouse relaxation time calculated using the procedure of Menezes and Graessley.[6,12]

treated using the bead grafting approach described by Sanchez-Reyes and Archer. The effectiveness of the procedure for reducing interfacial slip errors is independently evaluated from step shear measurements at multiple gap angles.

2. Experiment

An ultrahigh molecular weight, narrow molecular weight distribution polystyrene, PS20M, $\overline{M_w} = 20.06 \times 10^6$ g/mol and $\overline{M_n} = 16.72 \times 10^6$ g/mol, was purchased from Tosoh Corp., Japan. Solutions of PS20M in diethyl phthalate (DEP, Aldrich) were formulated using dichloromethane (methylene chloride, Aldrich) as cosolvent. PS/DEP solutions were prepared over a 3 month period to ensure homogeneity and complete cosolvent removal. Concentrations and degree of entanglement $N/N_e = (\overline{M_w}\varphi^{1.3})/M_{e0}$ information for all materials used in the study are summarized in Table 1. The entanglement molecular weight of polystyrene determined by Onogi and co-workers, $M_{e0} = 18\,000$ g/mol,[13] is used throughout.

Linear viscoelastic properties of the PS/DEP solutions were determined at 28.5 °C using a Rheometrics Ares rheometer (ARES) and a Paar Physica modular compact rheometer (MCR) equipped with 50 mm diameter titanium cone-and-plate fixtures (gap angle 1° and 2°). Oscillatory shear flow measurements were performed using bare fixtures as well as fixtures treated with a single layer of 10−30 μm diameter glass beads. Glass bead diameters in this range were selected on the basis of separate gap-dependent parallel plate steady shear experiments, which showed that slip violations in highly entangled PS/DEP solutions could be virtually eliminated using fixtures grafted with these beads.[11] The 10−30 μm beads were attached to the cone-and-plate fixtures used in the current study by a three-step process. In the first step a uniform thin film (ca. 4 μm) of a slow-cure epoxy adhesive was roll-coated onto the surface using glass rods. Following application, the epoxy film was partially cured at room temperature for several minutes. In the second step, a large excess of glass beads with the specified diameters was poured onto the partially cured adhesive, and the fixtures were cured at elevated temperature for periods of 5−48 h. In the final step, a high-pressure air stream was used to remove excess beads from the surfaces. The surface roughness of the fixtures was characterized using a Tencor Alpha Step 500 profilometer. The total roughness (peak-to-valley separation) of the unmodified titanium fixtures was $\Delta_t = 2.3$ μm and root-mean-squared roughness $\Delta_q = 0.5$ μm. The equivalent roughness measures for the bead-grafted surfaces are $\Delta_t = 36.8$ μm and $\Delta_q = 8.5$ μm.

The true gap angles α of bead-grafted shear fixtures were calibrated using small-amplitude oscillatory shear and step shear measurements on bare and surface modified cone-and-plate fixtures. Calibration experiments were performed using the lowest concentration solution PS20M1.5%, for which the validity of the no-slip boundary condition is most certain. The calibration measurements revealed that attachment of 10−30 μm glass beads increases α by between 0.04° and 0.1° with the largest changes at the smallest gap angles. Frequency-dependent storage and loss moduli obtained at 28.5 °C using fixtures with the two lowest gap angles (i.e., where errors due to surface roughness should be largest) are provided for PS20M5% and PS20M2.5% in parts a and b of Figure 1, respectively. These measurements were performed at nominal strain amplitudes of 2% and 10%, respectively. As expected, both figures show little, if any, effect of cone angle and

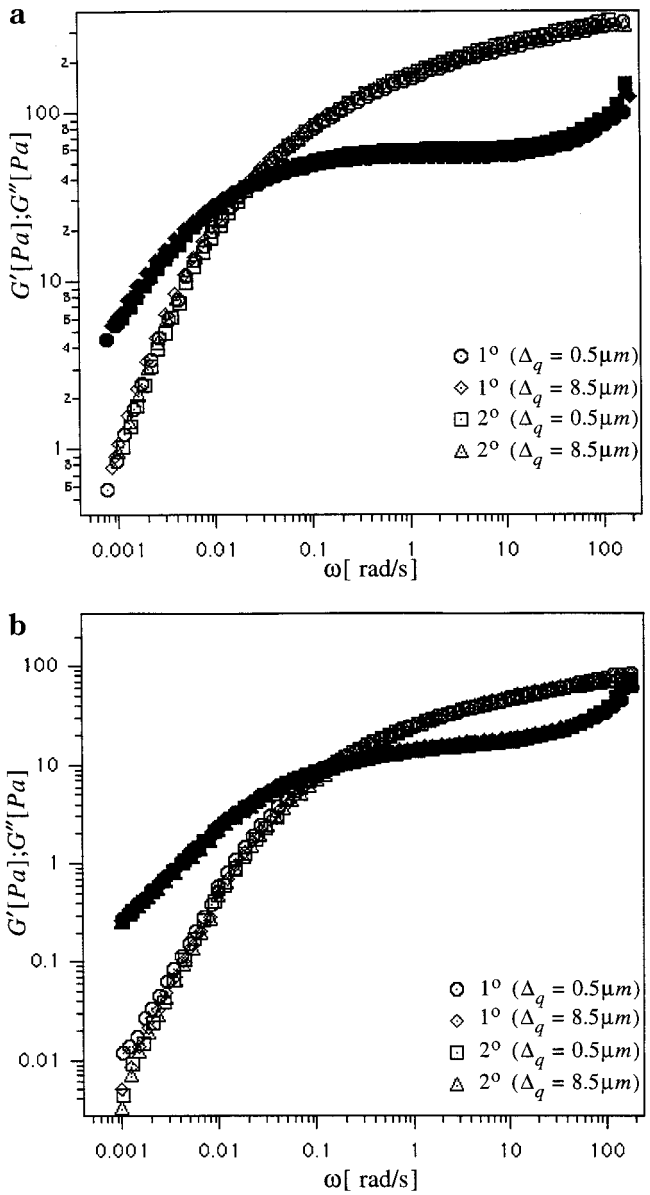

Figure 1. (a) Dynamic storage $G'(\omega)$ (filled symbols) and loss moduli $G''(\omega)$ for PS20M5% at 28.5 °C. Measurements were performed using 50 mm diameter titanium cone-and-plate fixtures roughened (Δ_q: root-mean-squared surface roughness) to minimize wall slip. Two gap angles 1° ("smooth" [circles] and roughened [diamonds]) and 2° ("smooth" [squares] and roughened [triangles]) were used to perform the measurements. (b) Dynamic storage $G'(\omega)$ (filled symbols) and loss moduli $G''(\omega)$ for PS20M2.5% at 28.5 °C. Measurements were performed using 50 mm diameter titanium cone-and-plate fixtures roughened (Δ_q: root-mean-squared surface roughness) to minimize wall slip. Two gap angles 1° ("smooth" [circles] and roughened [diamonds]) and 2° ("smooth" [squares] and roughened [triangle]) were used to perform the measurements.

roughness on the measured storage and loss moduli. Repeat experiments performed using polymer solutions sandwiched between the fixtures for durations as large as 1 week (the longest durations studied) showed no change in fluid properties or in bead structure at the surface, indicating that the surface modification is stable under the conditions of our experiments.

Zero-shear viscosities η_0 determined from the oscillatory shear measurements are tabulated in Table 1 for all but the most highly entangled solution, PS20M8%. For this material η_0 was obtained from steady shear flow measurements at low shear rates $\dot{\gamma} \ll \tau_d^{-1}$. Terminal times τ_d provided in the tables were determined from the long-time slope of plots of ln $G(t)$ vs t following imposition of small-amplitude step strain. In a few cases it was also possible to extract steady-state recoverable compliance J_e^0 values from low-frequency oscillatory shear data, allowing the weight-average terminal relaxation time $\tau_{d0,w} = \eta_0 J_e^0$ to be computed. Terminal times obtained using this procedure were lower by a factor ranging from 1.5 to 2 than those determined from step shear measurements. G_e values were obtained from the instantaneous $G(t)$ response following imposition of shear. These values compare favorably with plateau moduli estimated from storage moduli data at the loss minimum.

Nonlinear step shear measurements were performed at 28.5 °C using the MCR equipped with bead-grafted cone-and-plate fixtures. Nominal gap angles of 1°, 2°, 3°, and 5° were used to independently evaluate the effectiveness of the bead-grafting technique for reducing slip. The time required to impose nonlinear shear strains varied from 0.1 s, for the lower solution concentrations, to 0.15 s, for the highest polymer concentrations studied. These strain imposition times are more than 2 orders of magnitude lower than the terminal times for all but one of the materials studied and even in that case is approximately 60 times lower than τ_d, indicating that it is appropriate to consider the imposed deformation a step strain. Rest times of 8−10 times the terminal relaxation time were provided for stress relaxation between successive step strain measurements to minimize history effects on stress relaxation measurements. Strain amplitudes were sequenced in a random manner, with many repetitions, to isolate artifacts due to edge fracture and material expulsion from the gap at high shear strains. No evidence of either phenomenon was found in any of the polymer systems studied.

3. Results and Discussion

Nonlinear shear relaxation moduli $G(t;\gamma) \equiv \sigma(t,\gamma)/\gamma$ for the most highly entangled solution studied (PS20M8%, $N/N_e = 38$) are provided in Figure 2a for a range of shear strains. Time−strain factorability is evident at long times by visual comparison of $G(t;\gamma)$ at small and large shear strains. Factorability is confirmed by plotting $G(t,\gamma)h(\gamma)^{-1}$ vs time (Figure 2b). It is noteworthy that time−strain factorability is only approximate (i.e., $G(t,\gamma)h(\gamma)^{-1}$ data obtained at multiple shear strains do not collapse to a single line). But for the results at the largest strains, the overall shape of the $G(t,\gamma)h(\gamma)^{-1}$ plot is in fact very similar to results reported by Islam et al. for PS/DEP solutions of comparable entanglement density but sheared between smooth stainless steel cone-and-plate fixtures.[7] Specifically, the complicated crossing pattern in $G(t,\gamma)h(\gamma)^{-1}$ observed by these authors at high shear strains is reproduced here. Furthermore, the time λ_{k2} required for factorability is estimated to be 989 ± 185 s, which is at least a factor of 1.3 times larger than τ_d and nearly 3000 times larger than the longest Rouse relaxation time for the polymer,[6,12]

$$\tau_{\text{Rouse}} \approx \left(\frac{6}{\pi^2 \rho RT}\right) M_w^{2-\alpha} \frac{M_c^{\alpha-1}}{\phi^{(\beta(\alpha-1)+1)}} \eta_0[M_w, \phi] \approx 1.25 \text{ s}$$

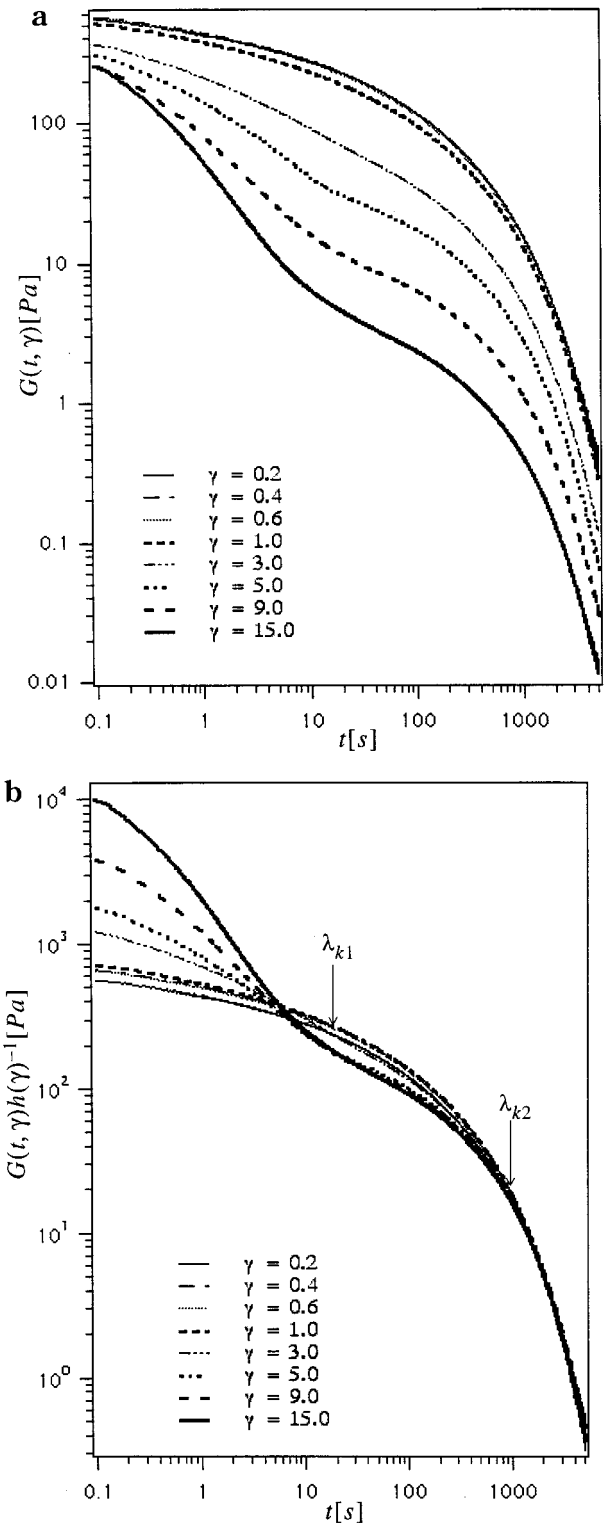

Figure 2. (a) Nonlinear shear relaxation modulus $G(t,\gamma)$ for PS20M8% at 28.5 °C. Shear strains γ ranging from 0.2 to 15.0 were used for these measurements. Strain increases from top to bottom in this figure. (b) Shifted nonlinear shear relaxation moduli $G(t,\gamma)h(\gamma)^{-1}$ for PS20M8% at 28.5 °C. The arrows in the figure locate the time λ_{k1} at which the fast relaxing component of $G(t,\gamma)$ becomes insignificant and the time λ_{k2} beyond which nonlinear moduli can be factorized (approximately) into separate strain- and time-dependent functions.

Here we have used $M_c = 33\,000$ g/mol, $\alpha = 3.7$, and $\beta = {}^4/_3$.[1,7] This estimate of τ_{Rouse} is about 30% larger than the value estimated using the relation $\tau_{\text{Rouse}} = (6M_w\eta_0/\pi^2 cRT)(1.5M_e/M_w)^{2.4} \approx 0.84$ s, where $M_e = cRT/G_N$ is

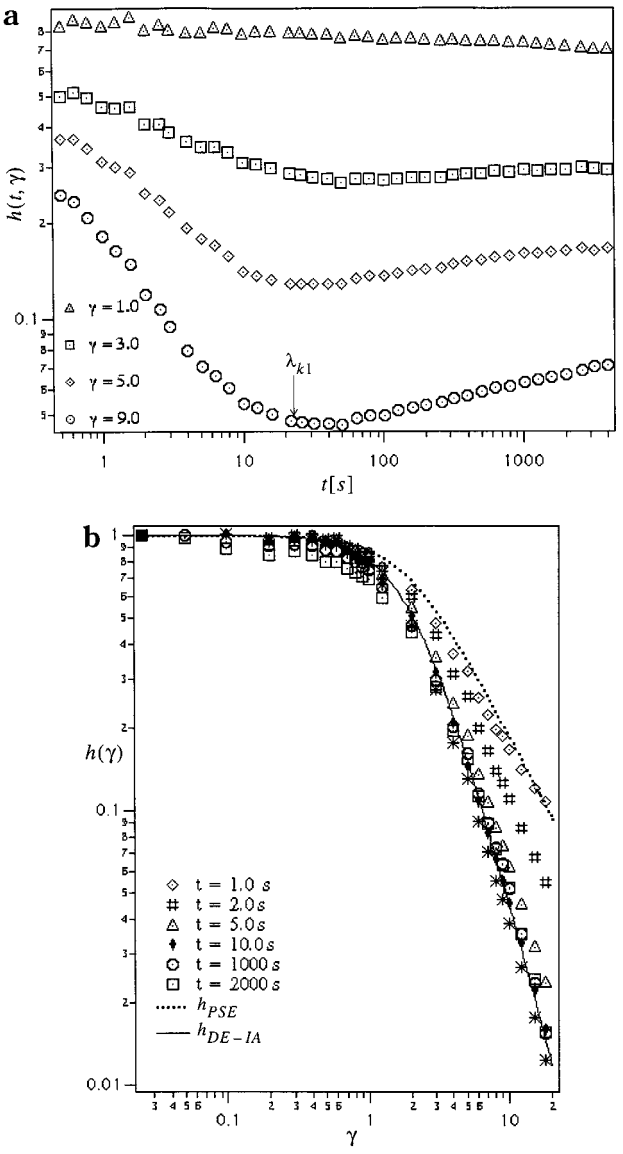

Figure 3. (a) Instantaneous shear damping function $h(\gamma)$ for PS20M8% at 28.5 °C. Solid line through the data is the damping function predicted by the Doi−Edwards theory with the independent alignment approximation.[2] The dashed line is the short time ($t \approx \tau_{Rouse}$) predicted by the partial strand extension model;[16] the long-time PSE damping function is close to h_{DE-IA}.[7] (b) Time-dependent shear damping function $h(t,\gamma)$ for PS20M8% at 28.5 °C at various shear strains. The arrow locates the time λ_{k1} at which $h(\gamma,t)$ appears to become independent of time (i.e., when $h(t,\gamma)$ is plotted on a linear scale).

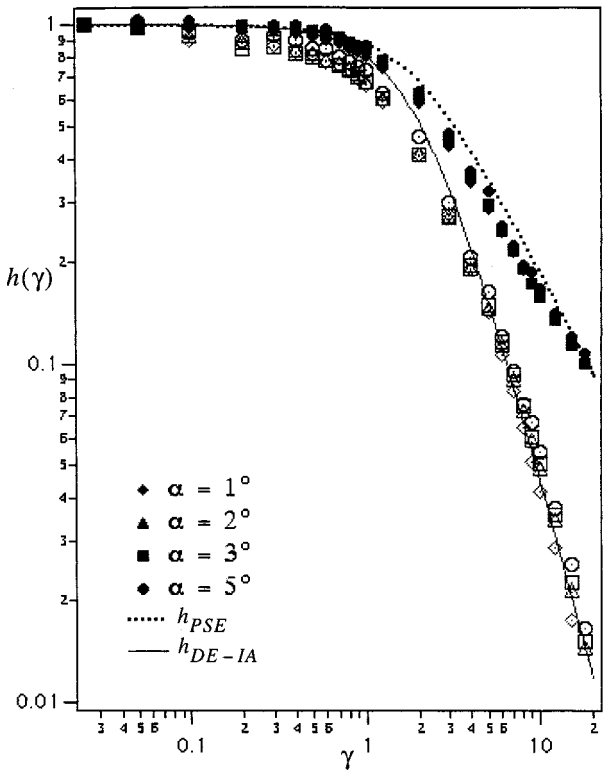

Figure 4. Long-time ($t > \lambda_{k2}$) and short-time ($t = 1$ s) shear damping function $h(\gamma)$ for PS20M8% measured using cone-and-plate fixtures with four different gap angles α. All shear fixtures were roughened using 10−30 μm glass beads to minimize measurement artifacts due to wall slip.

determined directly from the plateau modulus for the solution.[14] Inoue et al. have recently shown that τ_{Rouse} computed using either of these two approaches is generally larger than estimates obtained by fitting high-frequency storage moduli data.[15] Such large discrepancies between separability time and longest Rouse relaxation time are consistent with previous experimental results[6,7] but disagree with expectations from theory.

A second estimate of the factorability time can be obtained by plotting $h(\gamma,t) \equiv G(t,\gamma)/G(t,\gamma^*)$ vs time (Figure 3a). Here $\gamma^* = 0.05$ but could in principle be any strain in the linear regime. Time−strain factorability is evidenced by absence of time dependence in $h(\gamma,t)$. At small shear strains ($\gamma \leq 1$), Figure 3a shows that $h(\gamma,t)$ is independent of time, irrespective of the imposed strain. At shear strains above unity $h(\gamma,t)$ initially decreases with time, but after some time manifests a gradual, but continuous, increase, particularly at large strains. The overall magnitude of the increase is, nonetheless, so small that if the data are presented on linear scales, $h(\gamma,t)$ appears to become independent of strain after a time of order $\lambda_{k1} = 22 \pm 5$ s $= 17\tau_{Rouse}$, i.e., close to the minimum in $h(\gamma,t)$. This second "factorability" time is also larger than the $\lambda_k = 4.5\tau_{Rouse}$ value suggested by theory. It is nonetheless evident from Figure 2b that λ_{k1} is close to the time where the large-γ, faster relaxing component of $G(t,\gamma)h(\gamma)^{-1}$ disappears. λ_{k1} therefore appears to be of similar physical origin to the Rouse stretch relaxation process suggested by theory.[2]

The corresponding shear damping function $h(\gamma)$ for PS20M8% is presented in Figure 3b at several discrete times. The solid line through the data, h_{DE-IA}, is the long-time damping function predicted by the Doi−Edwards theory with the independent alignment approximation. The dotted line is the short-time ($t \approx \tau_{Rouse}$) prediction from Mhetar and Archer, h_{PSE}; the long-time ($t > \lambda_k$) damping function predicted by these authors is h_{DE-IA}.[16] It is readily apparent from these plots that $h(\gamma)$ is in nearly perfect accord with h_{DE-IA} at $t = 10$ s $\approx 8\tau_{Rouse}$. At longer times, the agreement is still good at high strains but is not as good at low shear strains. These levels of disagreement are nonetheless dramatically lower than observed in previous studies of comparably entangled polymer liquids. On the basis of the greater attention devoted to reducing wall slip in the rheometer fixture designs used here, we suspect that the better agreement comes from a reduced influence of slip. This suspicion is confirmed by $h(\gamma)$ results obtained from measurements at multiple gap angles (see Figure 4). These results show that changing α by a factor of 5 produces at most a 10% change in the short-

time ($t = 1$ s) or long-time ($t = 1000$ s) shear damping functions. Additionally, the differences in $h(\gamma)$ observed at variable α are nonsystematic, which is inconsistent with expectations if slip at the cone and/or plate was their source. A similar lack of systematic gap dependence was observed in $G(t,\gamma)h(\gamma)^{-1}$ over the same α range, simultaneously confirming that slip does not play a significant role in our observations and that the bead-grafting procedure is an effective method for removing wall slip artifacts in PS20M8% solutions, the most highly entangled polymer liquid studied.

$G(t,\gamma)$ and $G(t,\gamma)h(\gamma)^{-1}$ data for PS20M2.5% ($N/N_e = 8$, $\tau_{Rouse} \approx 0.85$ s) are summarized in parts a and b of Figure 5, respectively. The $G(t,\gamma)h(\gamma)^{-1}$ results are clearly different from those of PS20M8% in several related respects. First, $G(t,\gamma)$ is factorable into separate strain- and time-dependent functions when the initial fast relaxation process ends. This is in fact precisely the result predicted by the Doi−Edwards constitutive theory[2] and is consistent with results reported by several previous authors for comparably entangled polymer solutions.[2−7] Second, the complicated crossing pattern evident in $G(t,\gamma)h(\gamma)^{-1}$ for the more highly entangled material is absent. Finally, time−strain factorability is more certain, $\lambda_{k2} = 7.6$ s, and is observed over a wider range of times. Together, these observations suggest that, following the fast "stretch" relaxation process, orientation relaxation proceeds by the same mechanism as at equilibrium.

Figure 6 depicts the corresponding $h(\gamma,t)$ results for this same polymer solution at various discrete shear strains. In this case, $h(\gamma,t)$ is observed to become virtually independent of time beyond $t = \lambda_{k1} = 9.5 \pm 1.1$ s at all strains (i.e., both procedures for evaluating time−strain factorability yield roughly the same separability time, as they should). A relationship between the λ_{k1} and the estimated longest Rouse relaxation time can again be written $\lambda_k \approx 11.2\tau_{Rouse}$. The corresponding short-time ($t = 0.6$ s) and long-time ($t = 13$ s) step shear damping functions for PS20M2.5% are shown in Figure 7. Comparisons with experimental results obtained at a lower cone angle $\alpha = 1°$ and with h_{DE-IA} and h_{PSE} are also provided in this figure. Again, the short-time damping function is seen to be in fair accord with h_{PSE}. The long-time damping function is also observed to be in good to excellent agreement with h_{DE-IA}.

We now consider the nonlinear step shear relaxation behavior of a third polymer solution, PS20M5%. This solution has an entanglement density ($N/N_e = 22$) and longest Rouse relaxation time ($\tau_{Rouse} \approx 1.27$ s) nearly identical to that of PS20M8%. $G(t,\gamma)h(\gamma)^{-1}$ results are displayed in Figure 8a. These results show many of the features identified in PS20M8%, including the complicated crossing pattern. However, the regime intermediate between the time of first crossing and the factorability time $t = \lambda_{k2} = 213 \pm 42$ s is noticeably narrower. Nonlinear relaxation dynamics of PS20M8% are evidently also intermediate between those of the moderately and highly entangled solutions. $h(\gamma,t)$ results obtained at two gap angles $\alpha = 1°$ and 5° are provided in Figure 8b. Though there are clear differences between the two results, these differences are again at most a few percent over a 5-fold change in the cone angle, indicating that slip errors are small. Both sets of results also reveal a minimum in $h(\gamma,t)$, particularly at high strains. The magnitude of the minimum is in fact larger for the larger cone angle, which is exactly opposite of what would be expected if wall slip or some other interfacial artifact was to blame.

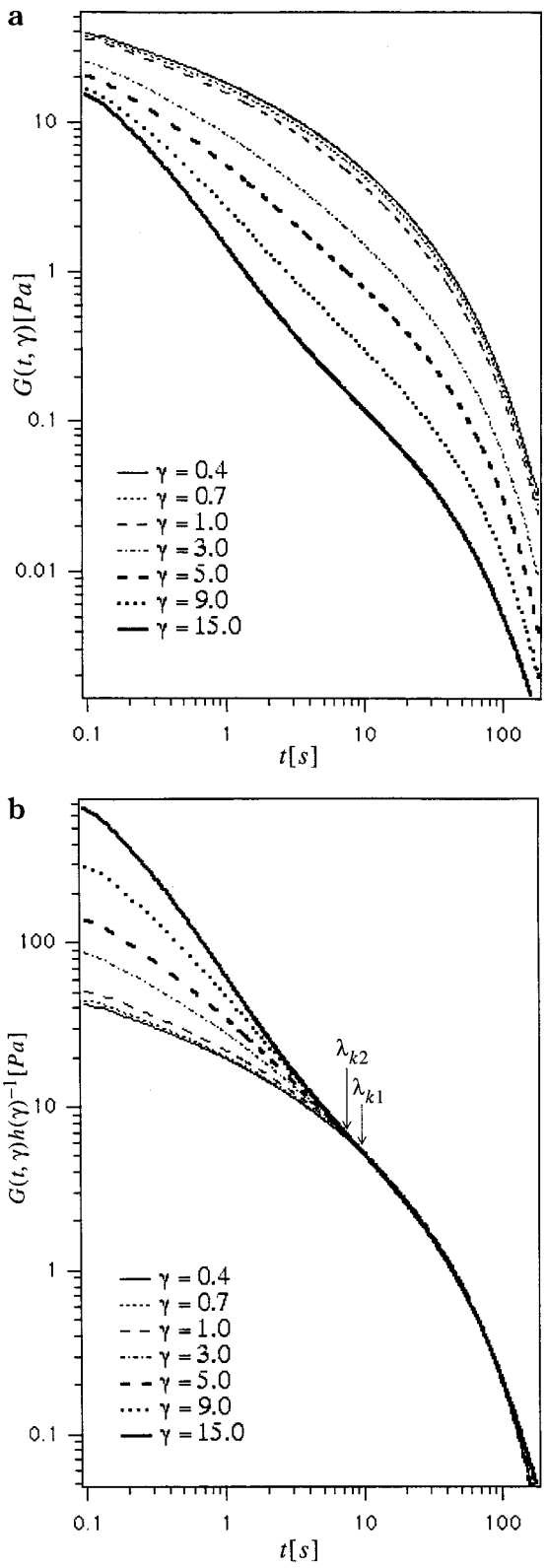

Figure 5. (a) Nonlinear shear relaxation modulus $G(t,\gamma)$ for PS20M2.5% at 28.5 °C. Shear strains γ ranging from 0.4 to 15.0 were used for these measurements. Measurements were performed using roughened 50 mm diameter, 5° cone-and-plate fixtures. Strain increases from top to bottom in this figure. (b) Shifted nonlinear shear relaxation moduli $G(t,\gamma)h(\gamma)^{-1}$ for PS20M2.5% at 28.5 °C. The arrows in the figure locate the time λ_{k1} at which the fast relaxing component of $G(t,\gamma)$ becomes insignificant and the separability time λ_{k2}.

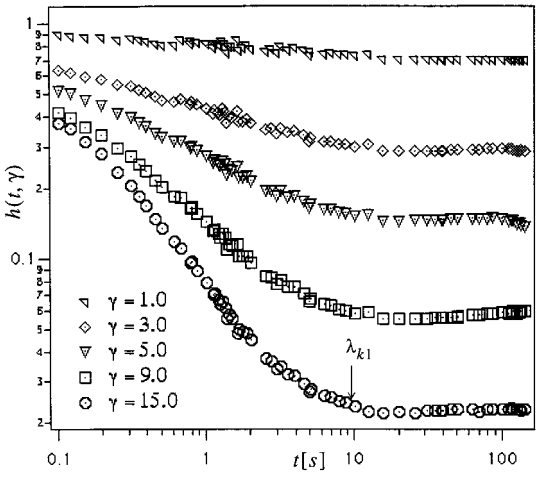

Figure 6. Time-dependent shear damping function $h(t,\gamma)$ for PS20M2.5% at 28.5 °C. The arrow locates the time λ_{k1} at which $h(t,\gamma)$ appears to become independent of time.

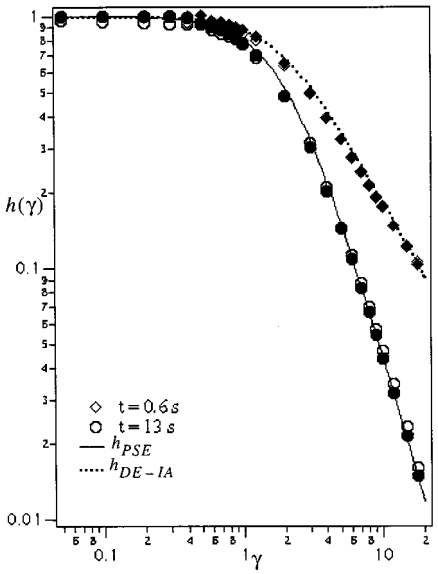

Figure 7. Short- and long-time shear damping functions $h(\gamma)$ for PS20M2.5% measured using 2° (filled symbols) and 2° (open symbols) cone-and-plate fixtures.

As in the case of PS20M8%, it is possible to estimate an apparent factorability time $\lambda_{k1} = 16 \pm 5$ s for this material by naively plotting $h(\gamma,t)$ vs time on linear scales and extracting the time at which $h(\gamma,t)$ appears to become independent of time. The relationship between λ_{k1} and the longest Rouse relaxation time is similar to the previous observations $\lambda_{k1} \approx 12.6\tau_{\text{Rouse}}$. This estimate of the separability time is also close to the time at which $h(t,\gamma)$ displays a local minimum at high strains, providing support for the idea that λ_{k1} is the time required for the faster "stretch" relaxation process to end. Short-time ($t = 0.5$ s) and long-time ($t = 200$ s) damping functions for PS20M5% obtained using four different cone angles are provided in Figure 9. The short-time $h(\gamma)$ results show very little, if any, dependence on α. The long-time damping function does show a dependence, but the effect is again quite weak and is also not systematic. Small negative deviations from $h_{\text{DE-IA}}$, similar to those seen in PS20M8%, are also observed for PS20M5%, particularly at low shear strains. The source of these discrepancies is unknown at the present time.

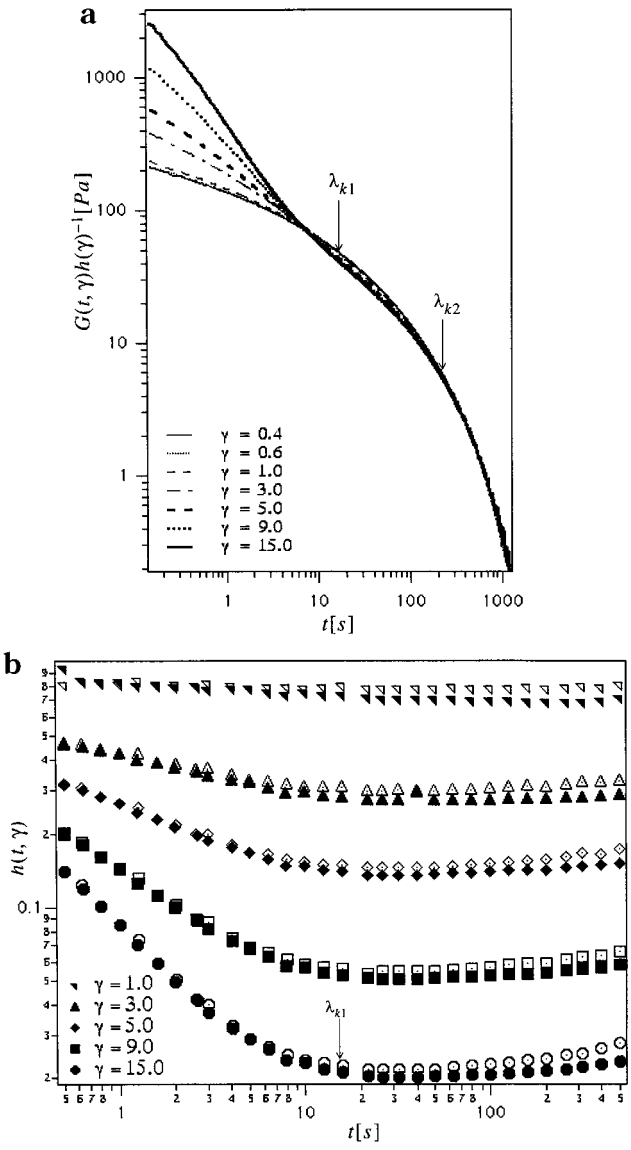

Figure 8. (a) Shifted nonlinear shear relaxation moduli $G(t,\gamma)h(\gamma)^{-1}$ for PS20M5% at 28.5 °C. Measurements were performed using roughened 50 mm diameter, 5° cone-and-plate fixtures. The arrows in the figure locate the time λ_{k1} at which the fast relaxing component of $G(t,\gamma)$ becomes insignificant and the separability time λ_{k2}. (b) Time-dependent shear damping function $h(t,\gamma)$ for PS20M5% at 28.5 °C. Results were obtained using 5° (open symbols) and 1° (filled symbols) cone-and-plate fixtures. The arrow locates the time λ_{k1} at which $h(t,\gamma)$ appears to become independent of time.

The main results of the paper are presented in Figures 10 and 11. In Figure 10 we plot the long-time ($t > \lambda_k$) damping function for PS/DEP solutions spanning the range from weakly entangled to well-entangled polymer liquids. Except for PS20M1.5% and PS20M2.5%, the results were obtained using 50 mm diameter cone-and-plate fixtures α = 3°, roughened by attachment of 10−30 μm glass beads. $h(\gamma)$ for PS20M1.5% and PS20M2.5% were obtained using cone-and-plate fixtures, roughened in the same manner, but with α = 1°. In agreement with earlier results reported by Archer,[6] and contrary to the observations reported by Islam et al.,[7] we find that the damping function does not show a systematic dependence on polymer entanglement density. Further, only modest negative deviations from $h_{\text{DE-IA}}$ are seen at low strains, even for the most highly entangled polymer solutions studied. These results

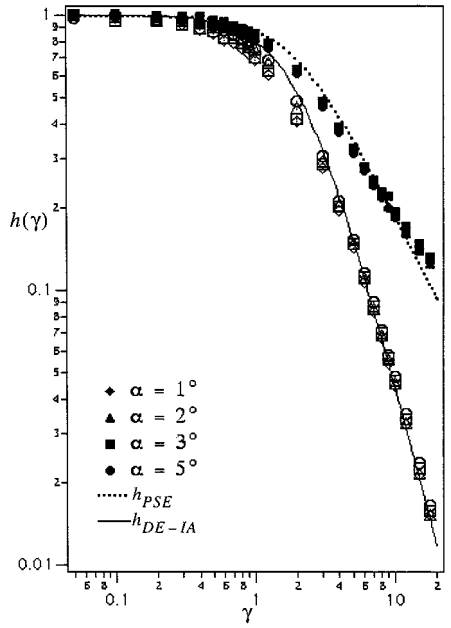

Figure 9. Long-time ($t > \lambda_{k2}$) and short-time ($t = 0.8$ s) shear damping function $h(\gamma)$ for PS20M5% measured using roughened cone-and-plate fixtures with four different gap angles α. These results indicate that wall slip has a minimal influence on $h(\gamma)$.

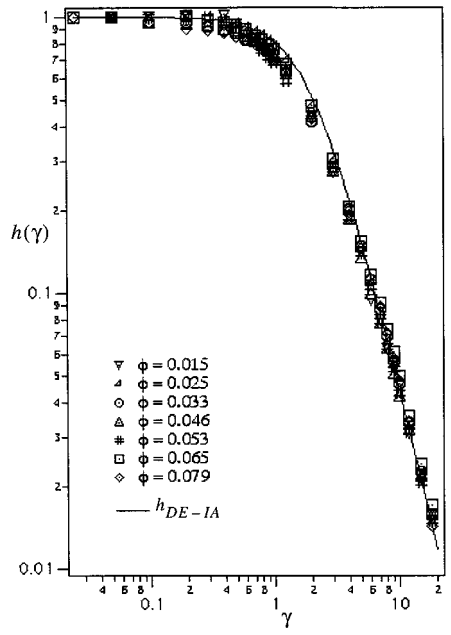

Figure 10. Long-time ($t > \lambda_{k2}$) shear damping function $h(\gamma)$ for all PS/DEP solutions studied. Except for the two lowest solution concentrations, measurements were performed using roughened 3° cone-and-plate fixtures; 1° fixtures were used to determine $h(\gamma)$ at the two lowest solution concentrations. The solid line is the damping function predicted by the Doi–Edwards theory with the independent alignment approximation.

therefore provide conclusive evidence in support of a single universal damping function for fluids in the class entangled polymer liquids.

The effects of polystyrene volume fraction on terminal and step shear properties of all solutions studied are summarized in Figure 11; the actual data are tabulated in Table 1. A strong correlation between τ_d and λ_{k2} is readily apparent from the experimental results. Linear fits to the data support the following scaling relationships: $\eta_0 \sim \phi^{4.7}$, $\tau_d \sim \phi^{2.7}$, $\lambda_{k1} \sim \phi^{0.65}$, and $\lambda_{k2} \sim \phi^{3.2}$. The longest Rouse relaxation time would be expected to scale with polymer volume fraction as $\tau_{Rouse} \sim \phi^{0.1}$ for the systems studied here. This result is also consistent with the longest Rouse times calculated from the zero-shear viscosities of the respective polymer solutions (see Table 1). Thus, the true separability time, evaluated from approximate overlap of $G(t,\gamma)h(\gamma)^{-1}$ data, appears to have very little to do with the longest Rouse relaxation time. The similarity of the concentration dependence of τ_d and λ_{k2} in fact mirrors the molecular weight dependences of these same properties recently reported for PS/DEP solutions with fixed concentrations.[6]

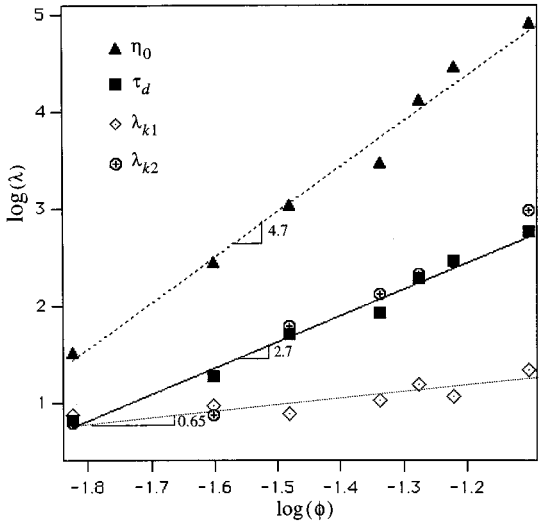

Figure 11. Effect of concentration ϕ on terminal properties and separability time of PS/DEP solutions. The best-fit straight lines through the data support the following relations: $\eta_0 \sim \phi^{4.7}$, $\tau_d \sim \phi^{2.7}$, and $\lambda_{k1} \sim \phi^{0.65}$.

More detailed consideration of the effect of solution concentration on viscoelastic properties can provide additional insight into the origin of the observed delay in time–strain factorability. Specifically, while the effect of concentration on zero-shear viscosity is close to previous results, $\eta_0 \sim \phi^{4.5\pm0.1}$,[1,17] none of the time scalings are consistent with expectations. This should be contrasted with the G_e data, which shows $G_e \sim \phi^{2.3}$, in near perfect agreement with the concentration scalings of plateau moduli $G_N \sim \phi^{1+a}$ and recoverable compliance $J_e^0 \sim \phi^{-(1+a)}$ found in previous studies;[1,17] here $a = 1.2 \pm 0.1$. A characteristic number-averaged terminal relaxation time $\tau_{d0,n} \approx \eta_0/G_e \sim \phi^{2.4}$, would therefore be anticipated. While it is tempting to attribute the stronger concentration scalings of τ_d and λ_{k1} to a concentration-dependent monomer friction coefficient, this conclusion is inconsistent with the lack of comparable enhancement in the concentration dependence of η_0 and τ_{Rouse} calculated from η_0. We suspect that this behavior is related to the even stronger effect of polymer concentration on λ_{k2} and perhaps even to the minimum in $h(\gamma,t)$ seen in solutions with $N/N_e \geq 11$.

Previous theoretical studies suggest that the postretraction entanglement structure in polymer liquids cannot be the same as at equilibrium. It has been contended, for example, that following retraction the average number of entanglements per polymer chain is reduced by a factor that depends on the size of the imposed strain in a model-dependent manner.[16] The mechanism by which entanglement structure is recovered is less certain. Several possibilities for tube recon-

struction following entanglement loss in nonlinear step shear have been considered previously.[16] Tube renewal was recently identified to be the most promising of these possibilities.[7] In particular, Islam et al. found that a transition from simple monotonic $G(t,\gamma)h(\gamma)^{-1}$, such as seen in PS20M2.5%, to more complex time dependencies such as in PS20M5% and PS20M8% can be predicted using tube models that accommodate gradual recreation of tube structure on time scales of order the constraint release time τ_{CR}. Even when this mechanism was included, the authors were unable to satisfactorily predict the large negative deviations from h_{DE-IA} observed experimentally. On the basis of the discussion in previous sections of this article, it now appears that this last failing was mostly a result of the unknown effect of wall slip on the experimental damping functions. That the complex crossing behavior in $G(t,\gamma)h(\gamma)^{-1}$ and delayed factorability are observed in the same range of solution entanglement densities, even after wall slip effects have been reduced, indicates that the proposed mechanism for entanglement recovery may still be plausible.

Experiments indicate that the constraint release time of long *P*-mer molecules relaxing in bidisperse blends with short *N*-mer chains scales with *P*, *N*, and N_e as $\tau_{CR} \approx N^{2.4\pm0.1}P^{2\pm0.2}N_e^{-2\pm0.3}$.[18] In a system of equal-sized molecules, τ_{CR} may therefore be related to τ_{d0} by $\tau_{CR} \sim (N/N_e)\tau_{d0}$. τ_{CR} is thus anticipated to be a stronger function of polymer concentration $\tau_{CR}(\phi) \sim \tau_{d0}(\phi)\phi^a \sim \phi^{2+a}$, which is sufficiently close to the result observed for λ_{k2} to indicate a possible influence of tube renewal on the longer factorability times measured. This statement is deliberately tentative because it is not substantiated by the molecular weight scalings of λ_k previously observed in PS/DEP solutions with fixed ϕ.[6] Furthermore, if λ_{k1} is indeed aligned with τ_{Rouse} as supposed, the stronger concentration dependences observed cannot be simply explained.

It is also evident from the data that some type of transition in $G(t;\gamma)$ occurs at or around $N/N_e = 8$. For polymers with entanglement densities below this value, the complicated crossing pattern in $G(t,\gamma)h(\gamma)^{-1}$ that appears to lead to delayed factorability is not seen but is readily observed even at N/N_e values as low as 11. This finding is in surprisingly good agreement with the observations of Islam et al.[7] A transition in relaxation dynamics near $N/N_e = 8$ is also evident from comparisons of the two "factorability" times; a clear separation in their magnitudes and concentration dependence in fact first becomes apparent just above $N/N_e = 8$.

4. Conclusions

Nonlinear step shear dynamics of polystyrene/diethyl phthalate solutions with entanglement densities N/N_e spanning the range from marginally entangled to well entangled were investigated by mechanical rheometry. Step shear experiments were performed using large-diameter cone-and-plate fixtures roughened with glass beads to minimize wall slip. The effectiveness of the surface roughening procedure was confirmed from rheological measurements at multiple gap angles. For all materials studied, $G(t,\gamma)$ could be visually separated into fast- and slow-relaxing components at large strain. The time λ_{k1} required for disappearance of the faster relaxing component can be related to the longest Rouse relaxation time τ_{Rouse} by $\lambda_{k1} = (12.9 \pm 1.8)\tau_{Rouse}$ for all PS/DEP solutions studied. The effect of polymer concentration on $\lambda_{k1} \sim \phi^{0.65}$ is, however, stronger than expected, $\tau_{Rouse} \sim \phi^0$, rendering the connection between the two time scales uncertain.

At times beyond a characteristic separability time λ_{k2}, nonlinear relaxation moduli $G(t,\gamma)$ of all solutions studied can be factorized into separate strain- and time-dependent functions. A relationship between λ_{k2} and the terminal relaxation time τ_d can be determined from the data, $\lambda_{k2} = (1.1 \pm 0.5)\tau_d$. However, the two time scales again depend on polymer concentration in rather different ways, $\lambda_{k2} \sim \phi^{3.2}$ and $\tau_d \sim \phi^{2.7}$. These observations should be contrasted with the concentration dependence of zero-shear viscosity $\eta_0 \sim \phi^{4.7}$ and elastic shear modulus $G_e \sim \phi^{2.3}$, which are both consistent with expectations for entangled PS/DEP solutions. The stronger concentration dependence of λ_{k2} can be rationalized in terms of a tube reorganization mechanism, characteristic relaxation time $\tau_{CR} \sim \phi^{3.2\pm0.1}$, for polymer reentanglement following nonlinear step strain.[7] Though this same process could influence the observed concentration dependence of τ_d, its effect at small step strains (i.e., where τ_d is determined) is unclear.

Step shear damping functions $h(\gamma)$ for PS/DEP solutions covering the range from marginally entangled to highly entangled are measured using 50 mm diameter cone-and-plate fixtures roughened with glass beads to reduce wall slip. The effectiveness of the roughening procedure for reducing slip is confirmed by nonlinear step shear measurements at multiple gap angles. These measurements show little, if any, effect of gap angle on $h(\gamma)$. Contrary to observations from several previous studies, we find little, if any, effect of N/N_e on long-time ($t > \lambda_{k2}$) $h(\gamma)$ in PS/DEP solutions. Specifically, for all systems studied $h(\gamma)$ is in good agreement with the damping function h_{DE-IA} predicted by the Doi−Edwards theory.[2] This finding provides convincing evidence in support of the universality of the step shear damping function for the class entangled fluids. The largest disagreements between $h(\gamma)$ and h_{DE-IA} are in fact observed at small strains, signaling an earlier onset of nonlinear shear response than envisioned by theory.

Acknowledgment. Support from the National Science Foundation Grants CMS-9713372 and CTS-0100579 is gratefully acknowledged. We are also grateful to Glen Swan of the Chemical Engineering machine shop for his assistance with the rheometer fixture designs used in the study.

References and Notes

(1) Ferry, J. D. *Viscoelastic Properties of Polymers*, 3rd ed.; Wiley: New York, 1980.
(2) Doi, M.; Edwards, S. F. *The Theory of Polymer Dynamics*; Oxford University Press: Oxford, 1986.
(3) Einaga, Y.; Osaki, K.; Kurata, M.; Kimura, S.; Tamura, M. *Polym. J.* **1971**, *2*, 550.
(4) Fukuda, M.; Osaki, K.; Kurata, M. *J. Polym. Sci., Polym. Phys. Ed.* **1975**, *13*, 1563.
(5) Osaki, K. *Rheol. Acta* **1993**, *32*, 429.
(6) Archer, L. A. *J. Rheol.* **1999**, *43*, 1555.
(7) Islam, M. T.; Sanchez-Reyes, J.; Archer, L. A. *J. Rheol.* **2001**, *45*, 61.
(8) Larson, R. G.; Khan, S. A.; Raju, V. R. *J. Rheol.* **1988**, *32*, 145.
(9) Morrison, F. A.; Larson, R. G. *J. Polym. Sci., Polym. Phys. Ed.* **1992**, *30*, 943.
(10) Vrentas, C. M.; Graessley, W. W. *J. Rheol.* **1982**, *26*, 359.

(11) Sanchez-Reyes, J.; Archer, L. A. *Langmuir*, submitted for publication.
(12) Menezes, E. V.; Graessley, W. W. *J. Polym. Sci., Polym. Phys. Ed.* **1982**, *20*, 1817.
(13) Onogi, S.; Masuda, T.; Kitagawa, K. *Macromolecules* **1970**, *3*, 109.
(14) Osaki, K.; Inoue, T.; Uematsu, T.; Yamashita, Y. *J. Polym. Sci., Polym. Phys. Ed.* **2001**, *39*, 1704.
(15) Inoue, T.; Yamashita, Y.; Osaki, K. *Macromolecules* **2002**, *35*, 1770.
(16) Mhetar, V. R.; Archer, L. A. *J. Non-Newtonian Fluid Mech.* **1999**, *81*, 71.
(17) Graesseley, W. W. *Adv. Polym. Sci.* **1974**, *16*, 1.
(18) Monfort, J. P.; Marin, G.; Monge, P. *Macromolecules* **1984**, *17*, 1551.

MA020321Q